Peer-reviewed version available at *Catalysts* **2018**, *8*, 430; doi:10.3390/catal8100430

High Pressure Photoreduction of CO_2: Effect of Catalyst Formulation, Hole Scavenger Addition and Operating Conditions

Elnaz Bahadori [a], Antonio Tripodi[a], Alberto Villa [a], Carlo Pirola [a], Laura Prati [a], Gianguido Ramis [b], Ilenia Rossetti [a,*]

[a] Dip. Chimica, Università degli Studi di Milano, INSTM Unit Milano-Università and CNR-ISTM, via C. Golgi, 19, I-20133 Milano

[b] Dip. di Ingegneria Civile, Chimica e Ambientale, Università degli Studi di Genova and INSTM Unit Genova, via all'Opera Pia 15A, I-16100, Genoa, Italy

Abstract

The photoreduction of CO_2 is an intriguing process, which allows the synthesis of fuels and chemicals. One of the limitations for CO_2 photoreduction in the liquid phase is its low solubility in water. This point has been here addressed by designing a fully innovative concept of pressurized photoreactor, allowing operation up to 20 bar and applied to improve the productivity of this very challenging process. The photoreduction of CO_2 in the liquid phase was performed using commercial TiO_2 (Evonink P25), TiO_2 obtained by flame spray pyrolysis (FSP) and gold doped P25 (0.2 wt% Au-P25) in the presence of Na_2SO_3 as hole scavenger (HS). The different reaction parameters (catalyst concentration, pH and amount of HS) have been addressed.

The products in liquid phase were formic acid and formaldehyde. Moreover, for longer reaction time and with total consumption of HS, gas phase products formed (H_2 and CO) after accumulation of significant amount of organic compounds in the liquid phase, due to their consecutive photoreforming. Enhanced CO_2 solubility in water was achieved by adding a base (pH= 12-14). In basic environment, CO_2 formed carbonates which further reduced to formaldehyde and formic acid and consequently formed CO/CO_2+H_2 in the gas phase through photoreforming. The

* Corresponding author: Fax +39-02-50314300; email ilenia.rossetti@unimi.it

deposition of small Au nanoparticles (3-5 nm) (NPs) onto TiO_2 was found to quantitatively influence the products distribution and increase the selectivity towards gas phase products.

Keywords: *CO_2 reduction; Photoreduction; Titania; Photocatalysis; High pressure photocatalysis.*

1 - Introduction

Carbon dioxide (CO_2) is one of the most important greenhouse gases emitted in the atmosphere and one of the main sources of global warming. According to the Intergovernmental Panel on Climate Change (IPCC 2001) Earth surface temperature has raised by approximately 0.6 °C in the past century. Accordingly, the Paris Agreement within 195 nations reached at COP21 in December 2015 was a major milestone capping more than two decades of global negotiations aimed at averting dangerous climate change and investments towards a low carbon, resilient and sustainable future.

Several studies have been focused on the activation of the very stable CO_2 molecule coming from carbon-capture and storage technologies (CCS) and converting it into useful chemicals for its valorisation [1]. The most interesting methods attempt the conversion of CO_2 into other useful compounds, *e.g.* regenerated fuels or chemicals, through chemical reactions [2], catalytic [3] and photocatalytic processes [4].

CO_2 is a relatively inert and stable compound, therefore its reduction by H_2O to form hydrocarbons is an "uphill" ($\Delta G > 0$) and strongly endothermic process, requiring a considerable amount of energy [5]. Photocatalysis seems to represent a valid and green method, which may exploit solar energy for sustainable reduction of CO_2 using water (H_2O) as both an electron donor and a proton source at low temperature and its conversion towards useful products, such as carbon monoxide (CO), formate, methanol, methane and oxygen (O_2) (Scheme 1) [6].

There are three main factors which play an important role in the photocatalysis process: solar light harvesting, separation of the photoproduced charges and surface reaction. Significant improvements have been achieved for optimization of the first 2 steps since they are based on the same issues as the widely studied solar driven water splitting. The major difference is the surface reaction of charge carriers [7,8]. In case of CO_2 photoreduction, surface reaction is more challenging due to severe competition with hydrogen evolution reaction (HER) in the presence of water, which is more abundant and preferentially adsorbed onto the catalyst surfaces than CO_2 [9,10]. Hence, design and fabrication of efficient photocatalysts for CO_2 reduction is the aim of several studies [7,10–13].

TiO_2, as a low cost semiconductor, resistant to photo-corrosion, has been widely studied for the adsorption, photoinduced activation and reduction of CO_2 [14–17]. He *et al.* proved that the anatase (101) facet played a critical role in CO_2 adsorption and assisting the electron transfer from

the surface of TiO_2 to CO_2 in the photoreduction process [18,19]. Besides, TiO_2, shows a favorable behavior toward generating and separating electron–hole pairs during photoexcitation [16]. However, in order to improve the catalyst efficiency, decreasing the bang gap and the fast recombination rate of holes and electrons generated during the irradiation process are the main concerns. To overcome this problem, various approaches have been developed: i) noble metals addition to TiO_2 acting as electron sinks (e.g. Au, Cu, Ag, Pd) [20,21], ii) the use of organic or inorganic hole scavengers (HS) to donate electrons to the valence band of the semiconductor preventing the accumulation of holes [11]. Even though, the use of HS has been shown to enhance the rate of the photocatalytic process, the by-products forming in their presence have to be also considered [22]. Sodium sulfite was chosen thanks to its ability to be oxidized into sulfate by the photogenerated holes and considered as a non-harmful, widely abundant compound [23].

We have already reported an innovative high pressure photoreactor, operating up to 20 bar [24,25] to successfully improve CO_2 solubility. The photoreduction reaction involves multiple proton-coupled electron transfer reactions and can lead to the formation of many different products, either in liquid phase: HCOOH, HCHO, CH_3OH or gas phase: H_2, CO, CH_4, depending on the reaction pathways, which makes this process rather complex (Scheme 1). A comparative study has been also carried out between the reaction in gas or liquid phase, the latter being the most promising [26] and leading to a promising rout for the storage of solar energy in form of organic molecules [27].

This work reports a comprehensive study on CO_2 photoreduction according to several variables. The reaction pathways and, thus, the control on products formation can be tuned by acting on different reaction parameters (e.g. pH, catalyst concentration and the amount of HS). Furthermore, improving the light harvesting capacity of TiO_2 by doping with Au nanoparticles, which also act as electron sinks, affected both productivity and products distribution. The photocatalytic activity of TiO_2 samples obtained by different preparation routes has been also investigated.

The specific configuration of the photoreactor suites the appropriate light distribution in the whole area. The very high productivity of H_2 and HCOOH even with bare P25 photocatalys with respect to previous studies on TiO_2 base photocatalyst, confirms the efficiency of our photoreactor.

Preprints (www.preprints.org) | NOT PEER-REVIEWED | Posted: 16 August 2018 doi:10.20944/preprints201808.0287.v1

Peer-reviewed version available at Catalysts 2018, 8, 430; doi:10.3390/catal8100430

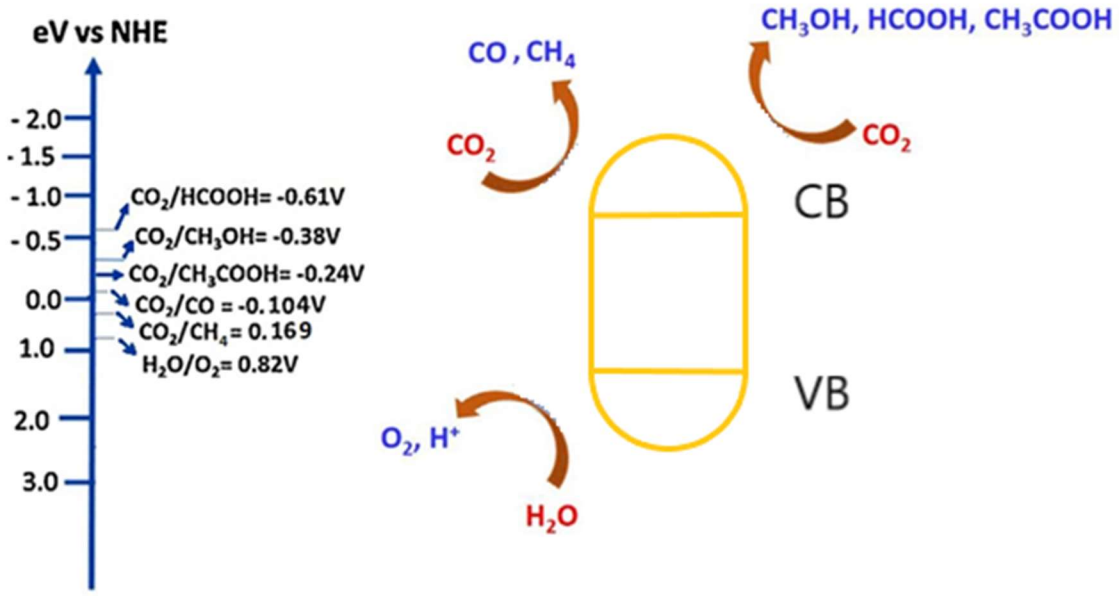

Scheme 1: Schematic illustration of different possible photocatalytic products formation during CO_2 photoreduction with H_2O over a heterogeneous photocatalyst and standard reduction potentials (V).

2 - Experimental

2.1 Materials Preparation

TiO_2 samples were prepared in dense nanoparticles form by FSP [28,29] and compared with a commercial P25 sample supplied by Evonik (code P25).

The FSP samples was prepared using a home-developed apparatus, composed of a burner which is co-fed with the titania precursor solution and 5 L/min of oxygen and the flame is ignited and sustained by a ring of flamelets (0.5 L/min CH_4 + 1 L/min of O_2). The solution of the oxide precursor in organic solvent is fed through a syringe pump at constant feeding rate of 2.5 ml/min in to the burner. The Titanium Isopropoxide (Sigma Aldrich, pur. 97%) as TiO_2 precursor was dissolved in o-xylene and Propionic acid (Sigma Aldrich, pur. 97%) with a 0.4 M concentration and injected through the burner. The pressure drop at the burner nozzle was 1.5 bar.

The gold doped TiO_2 samples (Au-P25) were prepared by a modified deposition-precipitation method using urea and a chemical reductant (DP-UC). 1g of commercial TiO_2 (Degussa P25, 50

m^2 g^{-1}) was dispersed in distilled water (100ml) then 5g of urea (Aldrich, >99%). $NaAuCl_4 \cdot 2H_2O$ solution (Aldrich, 99.99%) was added to the suspension and left under vigorous stirring for 4h at 80 °C. The catalyst was filtered and washed several times with distilled water. The collected sample after first washing was suspended in distilled water and a freshly prepared solution 0.1M of $NaBH_4$ (Fluka, >96%) was added ($NaBH_4$/Au = 4mol/mol) under vigorous stirring at room temperature. The sample was filtered, washed and dried at 100 °C for 4 h. Atomic Absorption Spectroscopy (AAS) analysis was (Perkin Elmer 3100 instrument) was performed to assess the final composition of Au-P25 catalysts: 0.2 wt% Au-P25, which proved the most active in a preliminary catalyst screening [30,31].

2.2 - Materials characterization

X-ray diffraction (XRD) analyses were performed by the Rigaku D III-MAX horizontal-scan powder diffractometer using the Cu-Kα radiation, with a graphite monochromator on the diffracted beam.

N_2 adsorption and desorption isotherms of samples were collected with a Micromeritics ASAP2020 apparatus.

Diffuse Reflectance (DR) UV-Vis spectra of samples were measured on a Cary 5000 UV-Vis-NIR spectrophotometer (Varian instruments) in the range of 200–800 nm.

TPR analysis was carried out on a bench scale apparatus by flowing 40 ml/min of a 10 vol% H_2/N_2 mixture, while heating the sample by 10 °C/min up to 700°C. The gas outflowing the quartz reactor was analysed by with a TCD detector after entrapping the possibly formed water.

2.3 - Photoreactor and testing conditions

All the experimental activity tests have been performed using an innovative pressurized batch photo-reactor which has been discussed in detail elsewhere [32,33]. The cylinder-shaped reactor made of AISI 316 stainless steel can operate up to 20 bar at temperatures up to 90°C. The temperature is kept constant through a double-walled thermostatic system. The internal capacity of the reactor is *ca.* 1.3 L, filled with *ca.* 1.2 L solution. Continuous stirring inside the reactor is provided by a magnetic stirrer placed underneath up to 400 RPM to ensure the optimal dispersion of the catalyst in the liquid phase.

The radiation source is a medium-pressure Hg vapour lamp with a range of emission between 254 nm $\leq \lambda \leq$ 364 nm, with maximum emission at this latter wavelength. An air circulation system has been used to cool the lamp. The power of irradiation directly depends on the flow rate of the cooling pressurized air. Therefore, the best cooling condition for the optimum lamp lifetime with the maximum irradiation power has been selected.

For the optimization of the best amount of catalyst, several concentrations have been chosen (*ca.* 0.5, 0.25, 0.125, 0.064, 0.031 g L^{-1}). The catalysts have been loaded with a suspension of bi-distilled water in the reactor. The best saturation condition has been settled overnight with the CO_2 saturation pressure of 7 bar and temperature of 80 ˚C, based on previous studies [24,32]. Testing was carried out under the same conditions, if not else specified. Such a pressure and temperature allow to obtain a broad products spectrum both in gas and liquid phase, so they were set as optimal to investigate the effect of other parameters on productivity and selectivity to all the products.

Na_2SO_3 has been used as HS in different amounts (*ca.* 1.66, 3.34, 6.68 g L^{-1}) to understand its effect on productivity and selectivity to the various products. As expected, negligible productivity both in liquid and gas phase has been observed without its addition. The photoreaction has been started by switching on the lamp for the 24 h of the reaction time.

Liquid products have been analyzed by taking samples at the end of the reaction. For analyzing the liquid products, HPLC (Agilent 1220 Infinity, with a column Alltech OA-10308, 300 mm_7.8 mm), equipped with both UV and refractive index (Agilent 1260 Infinity) detectors have been used. Aqueous H_3PO_4 solution (0.1 wt%) was used as the eluent. The gas products were collected in the headspace of the photoreactor and analyzed by a gas chromatograph (Agilent 7890) equipped with a TCD detector with the proper set up configuration for the quantification of H_2, CH_4 and polar/non polar light gases.

3 Results and discussion

3.1 - Materials characterization

The XRD pattern of TiO_2 sample obtained by flame pyrolysis shows a mixture of the crystalline phases of anatase and rutile with similar composition and particle size with respect to P25 samples (Table 1). All the reflections were identified by comparison with the standard JCPDS spectrum of rutile (file 88-1175) and anatase (file 84-1286) [34]. The phase composition and the average

particle of each sample have been estimated from the intensity ratio between the reflection of anatase and rutile planes at (101) and (110) respectively (Table 1) [35]. The particle size of TiO_2 samples has been calculated by using the Scherrer's equation [36].

The BET SSA (Brunauer-Emmett-Teller Specific Surface Area) and pore volume have been determined based on N_2 adsorption/desorption isotherms, collected at -196 °C for P25 and FSP samples, previously outgassed at 150 °C for 4h (Figure 1). Micropore volume was calculated according to the *t*-plot method (Table 1). Both P25 and FSP samples show a type II isotherm with H1 hysteresis loop, representing the agglomerates or spherical particles arranged uniformly with high pore size uniformity and facile pore connectivity [37]. FSP samples, however, show higher surface area and pore volume with respect to P2, which may positively affect its catalytic performance.

Table 1. Some relevant properties of the samples, as derived by N_2 sorption isotherms at -196 ºC, XRD patterns, and Band gap calculation from DR UV-Vis data elaborated according to Tauc plots

Sample	P25	FSP	0.2 wt% Au-P25
Anatase / Rutile (%)	78 / 22	69 / 31	78 / 22
Crystallite size [a]	15	20	15
BET Surface area (m^2g^{-1}) [b]	45	67	55
Total pore volume (cm^3g^{-1}) [c]	0.12	0.14	0.27
t-Plot micropore volume (cm^3g^{-1}) [c]	0.01	0.02	0.005
BJH Adsorption average pore width (nm)	22	20	31
Band Gap energy (eV) [d]	3.36	3.36	3.17

[a] Crystallite size quantification from XRD data through the Scherrer equation.
[b] as calculated from N_2 adsorption/desorption isotherms, collected at -196 °C
[c] as calculated by applying the t-plot.
[d] as calculated by the Tauc equation to DR-UV-Vis spectra

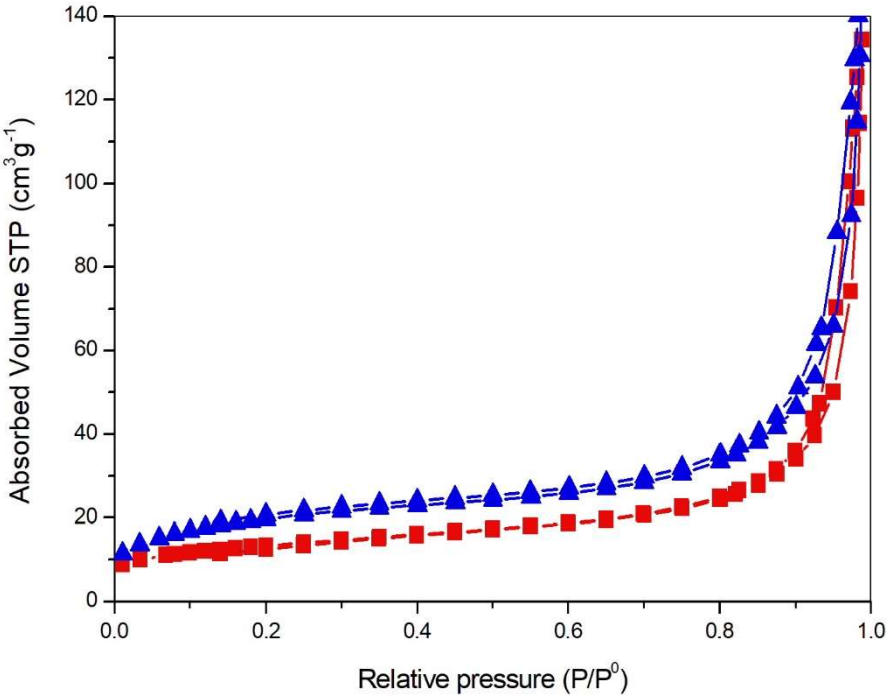

Figure 1: N_2 adsorption/desorption isotherms collected at -196 ºC over samples outgassed overnight at 150°C, P25 (squares), FSP (triangles)

According to UV absorption spectra (Figure 2a), both TiO_2 and Au-TiO_2 samples show an intense absorption in the spectral range between 240–380 nm, due to electron transfer from the 2p valence band orbital of O to the 3d conduction band orbital of Ti [38,39]. The spectra of un-doped TiO_2 samples show the cut-off at shorter wavelengths, with respect to the doped samples. The main reason for the observed bathochromic shift in transition and the visible light absorption is due to changing of the energy levels of the semiconductor band gap through a charge transfer between the metal conduction band and the valence band or the d–d transition in the crystal field [36].

In addition, the Au-TiO_2 sample exhibits significantly enhanced light absorption in the visible region showing a broad band located between 450 and 600 nm typical of the Surface Plasmonic Resonance (SPR) of Au nanoparticles (NPs) (*inset* of Figure 2a). The broad visible light absorption range is possibly due to wide size distribution of Au-NPs and the maximum of the SPR band (λ_{max}) intensity is mainly related to the size and content of Au particles.

Preprints (www.preprints.org) | NOT PEER-REVIEWED | Posted: 16 August 2018 doi:10.20944/preprints201808.0287.v1

Peer-reviewed version available at Catalysts 2018, 8, 430; doi:10.3390/catal8100430

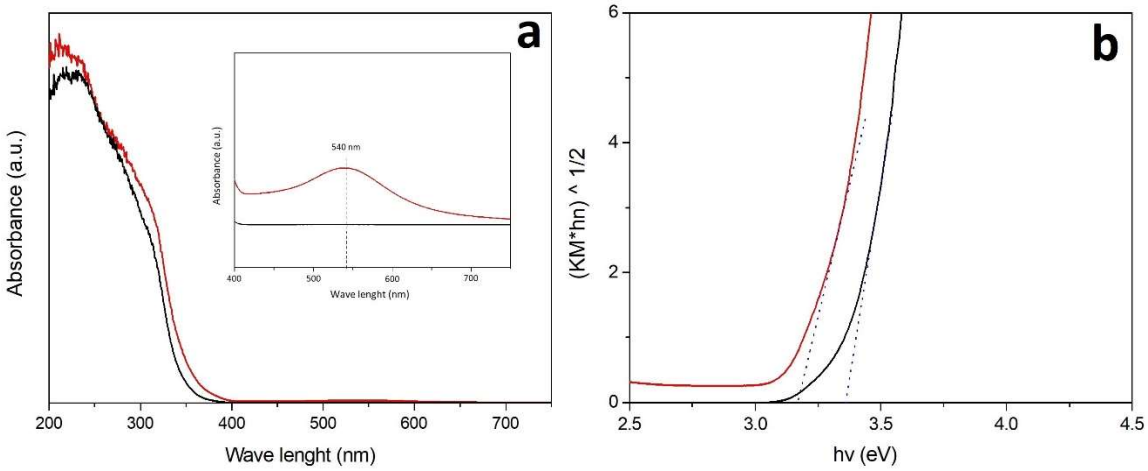

Figure. 2: DR UV-Vis spectra (left) and corresponding Tauc plots (right) of P25 (black curve) and promoted with Au (0.2 wt%; red curve)

The optical band gap energy E_g was determined according to the Tauc equation [40].

According to the E_g calculations (Figure 2b and Table 1) by promoting the TiO_2 samples with Au, the absorption has been extended to longer wavelengths and the band gap energy reduced [38,41].

3.2- CO_2 photo-reduction

3.2.1 - Effect of pH

The photoreduction of CO_2 may lead to a broad spectrum of products depending on photocatalyst formulation and reaction conditions, due to occurrence of many parallel and consecutive reaction steps [24,25,42].

The productivity and selectivity of products on P25 has been studied at pH 7.5 and 14 in the presence of 1.66 g L^{-1} HS (Figure 3). The productivity of the main products, HCOOH and H_2, increased in basic pH in fair agreement with previous observations [24,32]. Increasing the pH, improves the CO_2 solubility by forming CO_3^-or HCO_3^-, which further reduced to HCOOH or HCHO in a series of subsequent reactions (Scheme 2). Furthermore, the formed liquid products may evolve to gas phase products (H_2 and CO) due to the consecutive step of photo-reforming (Scheme 2) [24,32]. According to Ao *et al.,* [43] in studies at basic pH, the back-oxidation of HCHO to HCOOH is more likely.

Preprints (www.preprints.org) | NOT PEER-REVIEWED | Posted: 16 August 2018 doi:10.20944/preprints201808.0287.v1

Peer-reviewed version available at Catalysts 2018, 8, 430; doi:10.3390/catal8100430

No methane formation has been observed, since P25 as a photocatalyst is likely to produce CO or HCOOH, and is not likely to generate highly reduced hydrocarbons [44–47]. However, CO can be the precursor of methane formation following an alternative hydrogenation pathway [48].

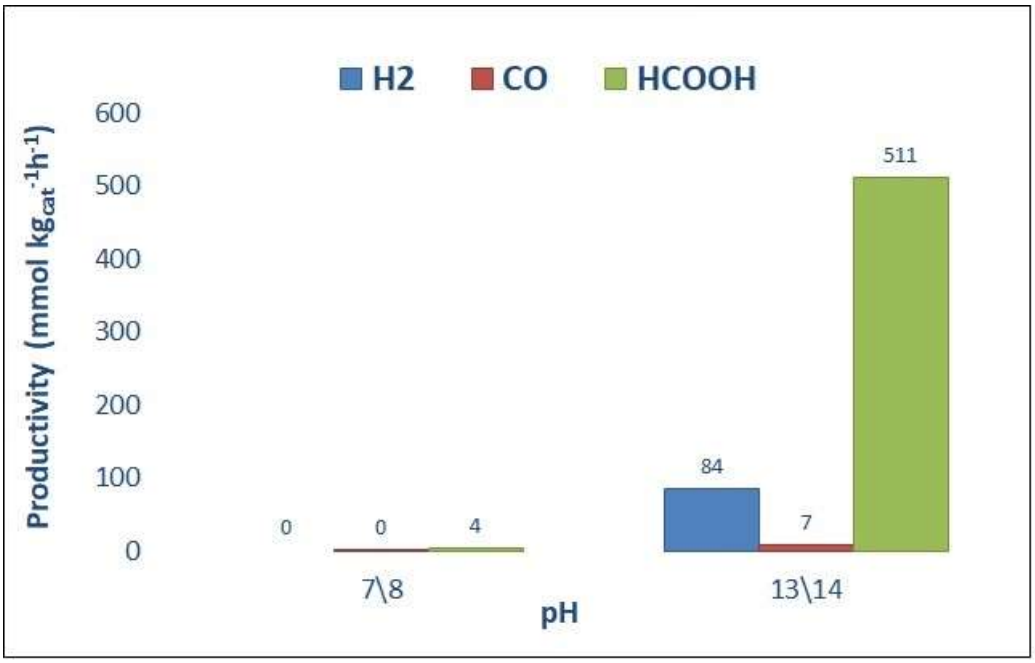

Figure 3: Influence of pH over productivity. Reaction conditions: 0.5 g L^{-1} of P25, 1.66 g L^{-1} HS.

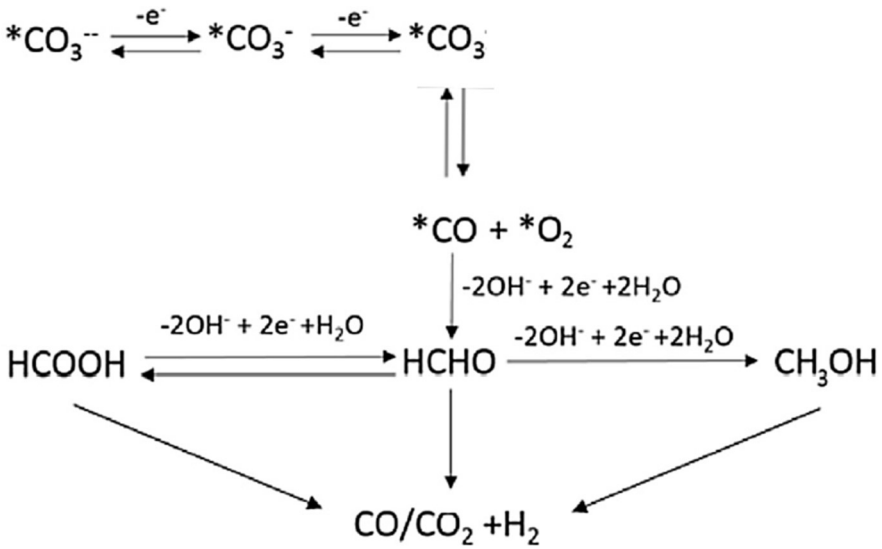

Scheme 2: Consecutive pathways for CO_2 photoreduction and photoreforming occurring at basic pH [32].

Peer-reviewed version available at Catalysts 2018, 8, 430; doi:10.3390/catal8100430

3.2.2 - Effect of catalyst amount

Optimization of catalyst amount has been performed decreasing progressively the catalyst concentration (0.5, 0.25, 0.125, 0.064 and 0.031 g L^{-1}) in the photoreactor by using the bare P25 catalyst. According to Figure 4, lower catalyst concentration increased productivity mainly due to better light distribution through the whole reactor. The productivity of the gas phase products (H_2 and CO) and of HCOOH, either normalized per mass of catalyst (Figure 4a) or not (Figure 4b) allowed to assess the best catalyst concentration in the slurry. 0.031 g L^{-1} of P25 returned the highest amounts of H_2 and HCOOH (Figure 4) per mass of catalyst. All the productivities decreased quite exponentially when increasing catalyst mass. When looking at the data without normalising against catalyst mass, the highest yield in HCOOH was obtained with the highest catalyst amount and progressively increased with increasing catalyst concentration. In a symmetric way, hydrogen and CO yields decreased progressively with increasing catalyst concentration (Figure 4b). Therefore, this parameter can be chosen to tune the process towards the maximisation of liquid or gas phase products.

0.031 g L^{-1} of catalyst was here taken as reference for further testing, so focusing on the highest gas phase productivity. Indeed, looking at the products distribution and intending this process as a mean to store solar energy by turning a waste greenhouse gas into useful compounds, we calculated the amount of energy stored in chemical form considering the different products we have obtained. We have taken as basis for calculation the enthalpy of combustion of HCOOH, H_2 and CO and made the calculation for the two extreme cases of catalyst concentration 0.031 and 0.5 g L^{-1} (Table 2). The amount of energy that is stored is slightly higher for the highest catalyst concentration and increases progressively with this parameter. However, the form of storage is different, as well as the easiness of separation and exploitation, which is likely better in the case of gas products than for the diluted liquid product. It is therefore possible to operate obtaining the highest yield of gaseous products, at low catalyst concentration, or to increase the liquid product yield with higher catalyst amount. In the following, we selected to use the lowest catalyst concentration, since it is more amenable for scale up and it leads to a balanced production of gas and liquid phase compounds, that allow to highlight the effect of the other operating parameters on reactivity.

Preprints (www.preprints.org) | NOT PEER-REVIEWED | Posted: 16 August 2018 doi:10.20944/preprints201808.0287.v1

Peer-reviewed version available at Catalysts 2018, 8, 430; doi:10.3390/catal8100430

Table 2: Amount of stored energy (kJ/h) in the form of different reaction products.

Chemically stored energy (kJ/h)						
		HS = 1.66 g/L				HS = 6.68 g/L
		P25		FSP	0.2 wt% Au/P25	P25
	Heat comb. (kJ/mol)	Cat = 0.031 g/L	Cat = 0.5 g/L	Cat = 0.031 g/L	Cat = 0.031 g/L	Cat = 0.031 g/L
HCOOH	254	0.036	0.066	0.069	0.066	0.372
H_2	286	0.034	0.011	0.018	0.021	0.005
CO	283	0.003	0.001	0.002	0.003	0.0003
Total	-	0.073	0.079	0.089	0.090	0.377

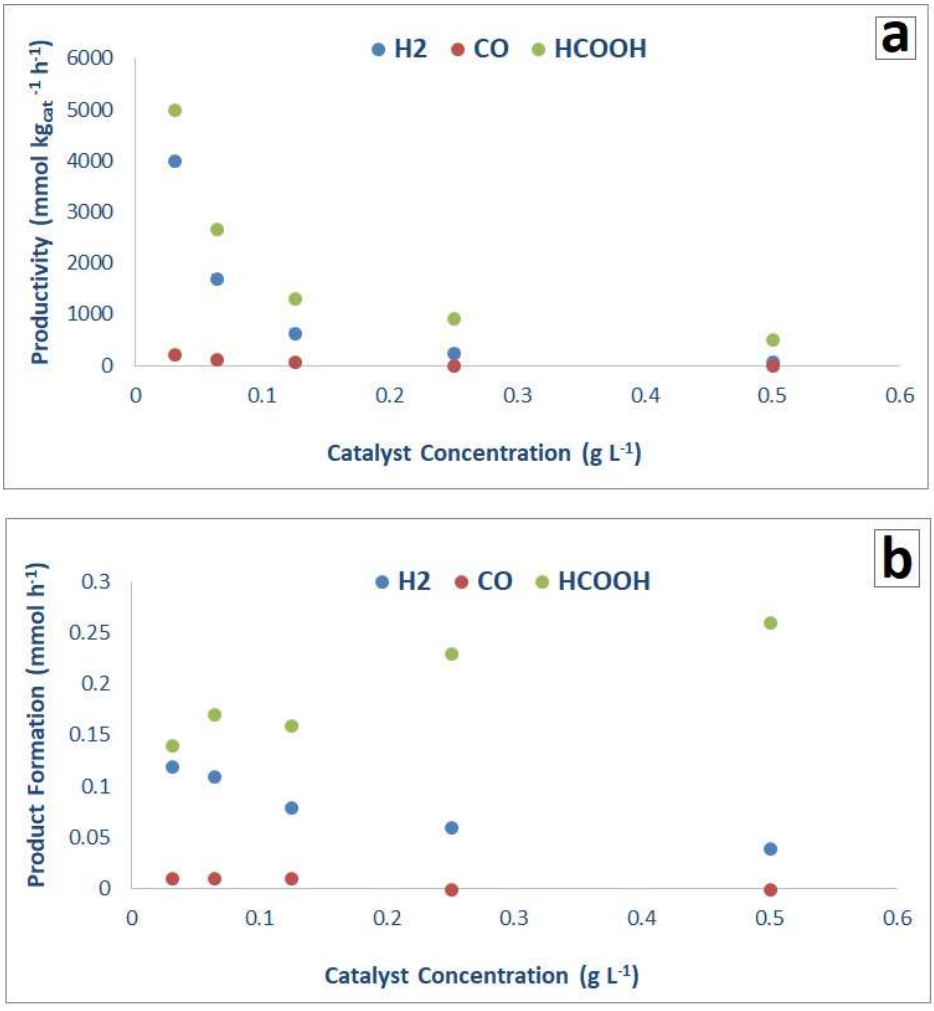

Figure 4: Effect of catalyst concentration on productivity (a) and absolute product formation (b) with the P25 as a catalyst (1.66 g L^{-1} HS)

3.2.3 - Effect of the hole scavenger (HS)

The efficiency of the photocatalyst is limited by the slow charge transfer, subsequent reactions of the photo-excited holes and the high charge recombination rates. In fact, consumption of conduction band electrons must be efficiently balanced by holes reduction. This process occurs in the presence of electron donor species, otherwise reaction rate is highly depressed.

Sodium sulfite (Na_2SO_3) was chosen as inorganic HS, added in different concentration (*ca*. 1.66, 3.34, 6.68 g L^{-1}) and its consumption was determined after reaction by iodometric titration. Negligible productivity has been observed without HS addition. Sodium sulfite is an inorganic and non-competing species, with a high performance in photocatalytic reactions [23]. Moreover, sodium sulfite can be industrially employed due to its low cost.

Figure 5 reports that increasing the HS concentration from 1.66 to 6.68 g L^{-1} (4-fold increase) increases the HCOOH productivity up to 9 times, whereas clearly decreasing the formation of gas products (H_2 and CO). The results of our previous studies already demonstrated that the formation of the gas phase products (H_2, CO, CH_4) starts after the consumption of the HS. Indeed, in absence of the sulphite the organic compounds accumulated in the reaction medium start acting as hole scavengers themselves through a consecutive photoreforming path (Scheme 2). Sulphites titration confirms the total consumption in 24 h of the base-case concentration 1.66 g L^{-1} (Figure 6). However, 24 hours of reaction time were not enough for the total consumption of the HS when loaded in higher quantity (3.34 and 6.68 g L^{-1}), which in turn inhibits the formation of gaseous products and favors the formation of HCOOH (Figure 6). This study supports the above proposed mechanism of the reaction and the role of HS (reaction time) on the selectivity to the different products.

Moreover, according to Table 2, the boosted productivity to HCOOH, which is unprecedented in previous reports on this reaction, allows to tune also HS concentration, in addition to catalyst one, to address the reaction towards the desired products. It may be noticed, indeed, that the test with the highest HS concentration led to the highest amount of stored energy, which increased by one order of magnitude the stored energy amount even by increasing its concentration by a factor of 4, only. The choice of its use should be determined on the basis of the desired reaction path. The increase of HS makes photoreduction essentially more effective when leading to HCOOH. Its further transformation to H_2 is inhibited until the complete consumption of the HS, leading to liquid phase products, only.

Preprints (www.preprints.org) | NOT PEER-REVIEWED | Posted: 16 August 2018 doi:10.20944/preprints201808.0287.v1

Peer-reviewed version available at Catalysts 2018, 8, 430; doi:10.3390/catal8100430

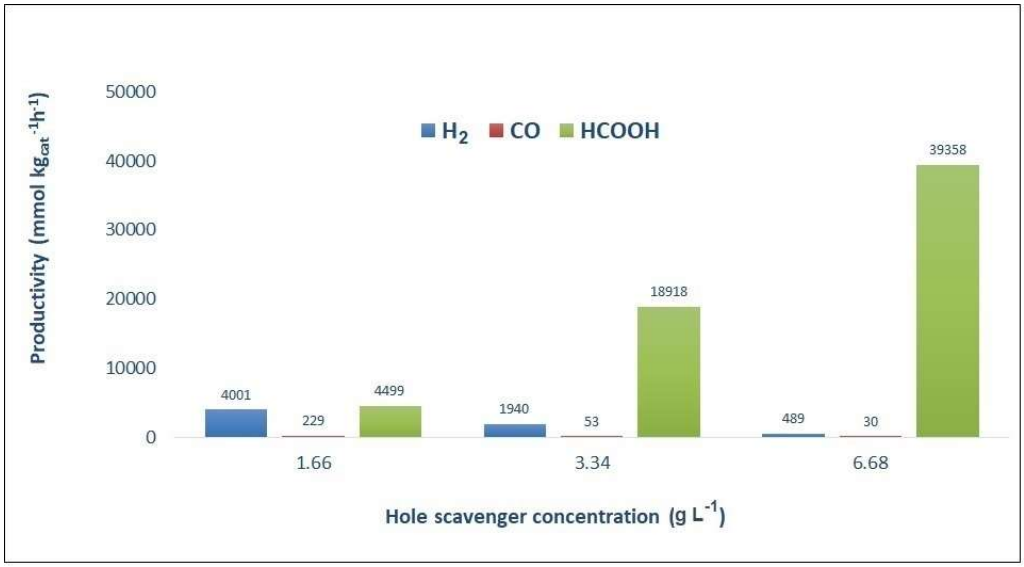

Figure 5: Effect of HS concentration on productivity. Reaction time: 24 h. P25 as a photocatalyst (0.031 g L^{-1}).

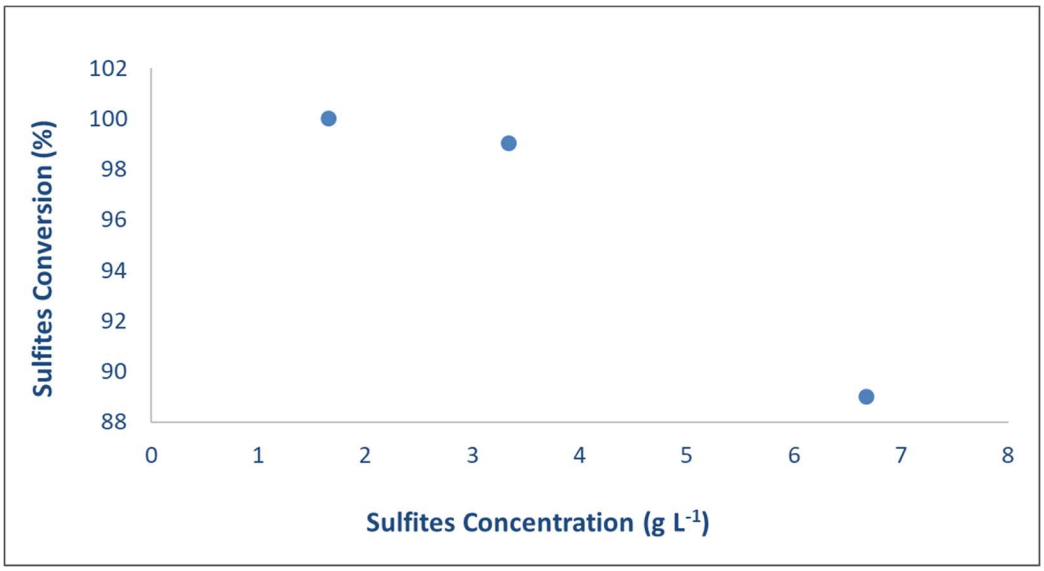

Figure 6: Sulfite conversion vs. their initial concentration after 24 hours of reaction. P25 as a photocatalyst with 0.031 g.L^{-1} loading

3.2.4- Comparison between different photocatalysts

Flame spray pyrolysis allows the synthesis of titanium dioxide nanoparticles characterized by high surface area and high thermal stability [28,49–51]. Due to the abundance of oxygen and high temperature in the FSP reactor, the nanoparticles produced by FSP are typically fully oxidized and highly crystalline. The simple synthesis procedure permits the rapid and continuous production of the catalyst.

FSP titanium dioxide prepared in our lab has been tested for comparison with the commercial P25 titania. The samples were compared using 1.66 g L^{-1} of HS, with the selected catalyst loading (0.031 g L^{-1}) at 2 different pH conditions (Figure 7). Also in this case the conditions were selected to obtain significant amounts of products in both liquid and gas phase to check the effect of the other variables on both the mechanisms.

The results confirm also for the FSP titania a very limited productivity at neutral pH and a good productivity at basic pH. Slightly higher productivity of FSP has been partly attributed to its higher surface area (67 m^2g^{-1} for FSP, 45 m^2g^{-1} for P25), which increases the surface reactions rate, though being almost indifferent as for the main photochemical steps. Furthermore, the quite high activity of FSP and P25 catalysts has been attributed to the enhanced charge separation at the anatase-rutile interface which acts as charge traps (hence higher capacitance). This effect is much more remarkable for FSP at low catalyst loading, compared to the commercial TiO_2 catalysts. According to previous studies [49,51], short flame residence time at extreme condition arising from high temperature may produce a metastable phase and also small concentration of defect states in the bandgap due to a Ti^{4+} stoichiometry deficiency, thus, enabling electron-hole pair generation as well as acting as photocharge trap defects [52]. The enhanced photocatalytic performance of FSP catalyst has been confirmed when varying catalyst concentration, which may result in an average smaller primary particles and agglomerates and decreases the light scattering (Figure 8) [49]. These results imply that the flame spray pyrolysis is a promising technique to produce catalyst that can be employed industrially for this application.

Preprints (www.preprints.org) | NOT PEER-REVIEWED | Posted: 16 August 2018 doi:10.20944/preprints201808.0287.v1

Peer-reviewed version available at Catalysts 2018, 8, 430; doi:10.3390/catal8100430

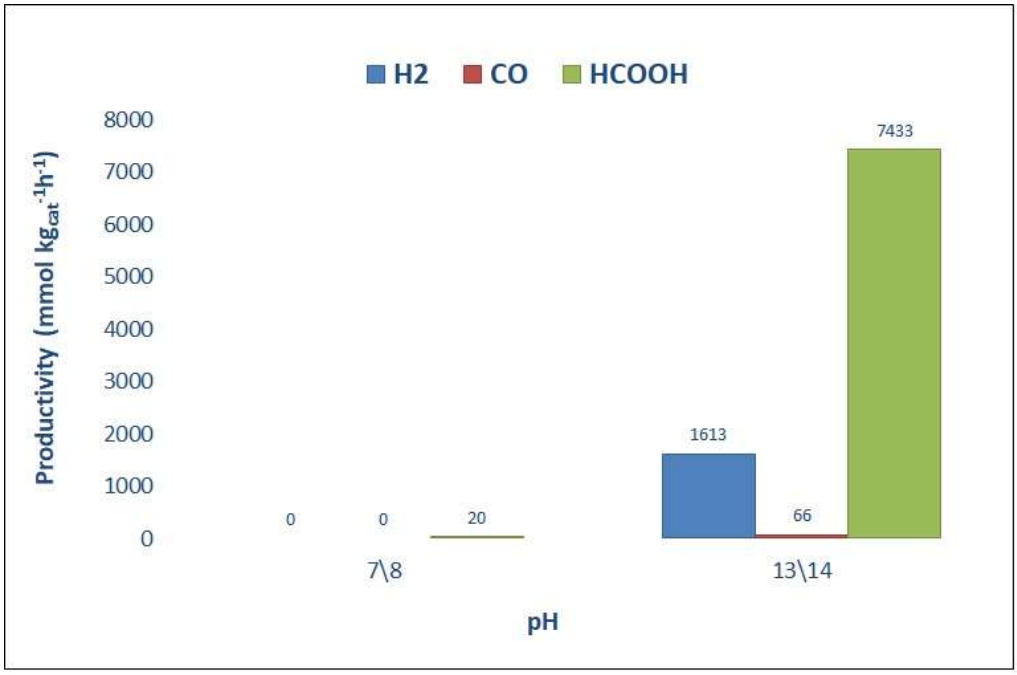

Figure 7: Influence of pH over productivity (0.031 g $L^{-1}$of FSP and 1.66 g L^{-1} HS).

Metals addition is a common strategy to improve visible light harvesting and to enhance the separation of photogenerated charges. We have deepened the performance of gold nanoparticles on the productivity and selectivity of products. 0.2 wt% Au loading was selected based on previous screening [32]. Au-P25 has been tested maintaining a fix value of HS 1.66 g L^{-1}, basic conditions (pH 13/14) and, also in this case, variable catalyst amount. Figure 8 reports the overall comparison of productivity of all the tested photocatalysts.

The comparison of different catalysts maintaining the highest catalyst concentration in the reactor (0.5 g L^{-1}), demonstrates that adding gold to P25 increases the selectivity towards secondary products (hydrogen and CO) with respect to bare P25 and even FSP. Gold doped catalyst is characterized by higher visible light absorption, which positively affects the light harvesting ability and consequently the overall productivity. Furthermore, gold may act as electron trap to improve the charge separation efficiency. This increases the photocatalyst effectiveness for all the reaction steps depicted in the reaction schemes (*vide supra*).

CO can be either obtained by *i)* direct photoreduction of CO_2, or *ii)* as a product of photoreforming of the organic compounds obtained in liquid phase by CO_2 photoreduction, or even *iii)* by catalytic reduction of CO_2 by using the photogenerated H_2. The productivity trend of CO and H_2 are so

Peer-reviewed version available at Catalysts 2018, 8, 430; doi:10.3390/catal8100430

similar to suggests that both species are produced by photoreforming of the primary organic products of photoreduction accumulated in the liquid phase.

On the contrary, for 0.2 wt% Au-P25 decreasing the catalyst concentration results in decreasing selectivity towards hydrogen production with respect to P25, balanced by a significant increase of the productivity to HCOOH (Figure 8). The enhancement of productivity is due to the strong electric fields created by the surface plasmon resonance of the Au nanoparticles, which excite electron-hole pairs locally in the TiO_2 and produces a number of additional photocatalytic reaction products at a rate several orders of magnitude higher than the normal incident light [52]. In this wavelength range, both the excited electrons in Au and TiO_2 contribute to the reduction of CO_2 with H_2O [52].

Overall, by calculating the amount of energy stored as in Table 2, there is no appreciable difference between the use of the FSP catalyst and the 0.2 wt% Au/P25 one, both being more efficient than P25 from this point of view.

Finally, Table 3 gives a comprehensive comparison of the different TiO_2 based photocatalysts used for CO_2 photoreduction and their productivity and selectivity, in comparison with the present work. The comparison with the relevant literature reports confirm the validity of the presently adopted high pressure photoreduction apparatus, which is able to overperform most results by various orders of magnitude.

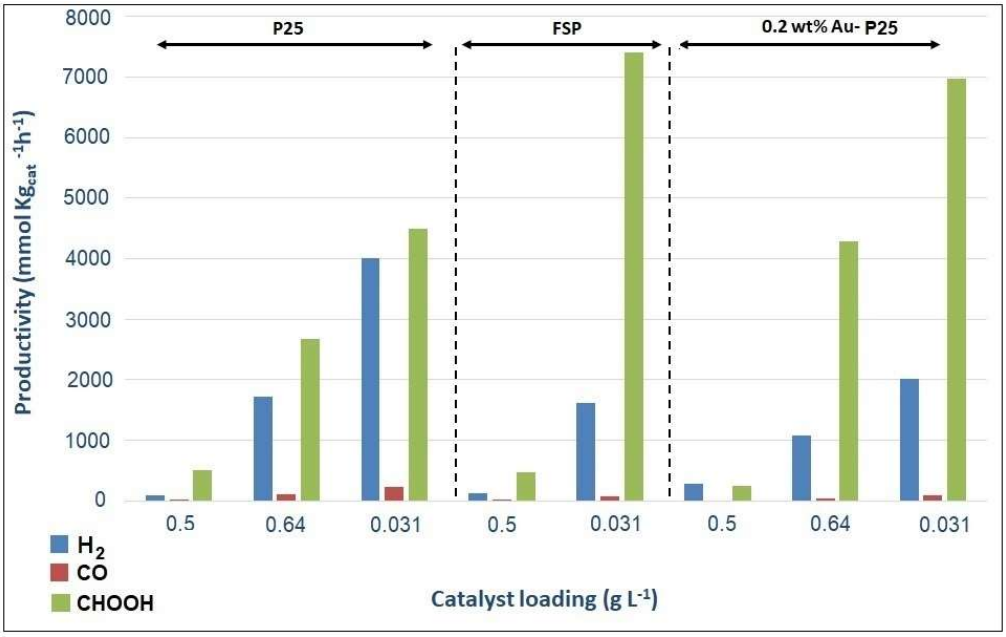

Figure 8: Products productivity with respect to different catalysts in different loadings with HS = 1.66 g L^{-1} and at pH = 13/14.

Preprints (www.preprints.org) | NOT PEER-REVIEWED | Posted: 16 August 2018 doi:10.20944/preprints201808.0287.v1

Peer-reviewed version available at Catalysts 2018, 8, 430; doi:10.3390/catal8100430

Table 3: Comparison of the photocatalytic performance for CO_2 photoreduction of TiO_2-based photocatalysts obtained with different techniques.

Strategy	Photocatalytis	Synthesis method	Reaction Condition	Reaction activity	Ref
Increasing Surface area	Structural controlling by Anatase TiO_2 with co-exposed (001) and (101) facets	Adjusting HF amounts in the solvothermal method	10 g L^{-1} catalysts. 300 W Xe arc lamp	The highest CH_4 generation rate was 1.35 µmol g^{-1} h^{-1} over HF4.5	[53]
Surface Defects	$Cu_{(I)}/TiO_{2-x}$ nanoparticles	Precipitation followed by thermal treatment	50 mg catalysts under 2 mL min^{-1} CO_2 flow; 150 W solar simulator (B90 mW cm^{-1})	$Cu_{(I)}/TiO_{2-x}$ exhibited the maximum CO production rate of 4.3 µmol g^{-1} h^{-1}	[54]
Surface basic sites	NaOH–TiO_2 composites	Impregnation method	80 mg catalysts in 80 kPa CO_2 with H_2O vapour; 300 W Xe lamp	With 3 wt% NaOH loading (NaOH–TiO_2) the maximum CH_4 formation was obtained with 52 µmol g^{-1} in 6 hours	[55]
	Pt–MgO/TiO_2	Photo deposition and impregnation methods	20 mg catalysts in 2.0 MPa CO_2 with H_2O vapour; 100 W Xe lamp (λ = 320–780 nm)	Pt-1.0 wt% MgO/TiO_2 exhibited the highest CH_4 amount of 2.2 µmol in 10 hours	[56]
	MEA-functionalized TiO_2	Solvothermal method	20 mg catalysts in 0.1 mL H_2O; Xe lamp	The catalyst exhibited CO and CH_4 generation amounts of 66.7 and 8.61 ppm h^{-1}, respectively	[57]
Surface noble-metal co-catalysts	3.0 wt% CuO loaded TiO_2	Impregnation and sonication	300 mg catalysts in 300 mL 1 M $KHCO_3$; CO_2 bubbled for 30 min; 10 W UV lamp (2.45 mW cm^{-1})	Methanol reached 442.5 µmol g^{-1} h^{-1}, 2.4 times higher than with P25 due to the lower activation energy	[58]
	Pd–TiO_2	Photochemical deposition	150 mg catalysts in 1.5 mL H_2O; 500 W Hg lamp with a filter (λ> 310 nm)	Pd–TiO_2 exhibited a preferential generation of CH_4 instead of CO for bare TiO_2	[59]
	Pt–TiO_2 columnar films	Aerosol chemical vapor deposition	The flow rate of CO_2 and water vapor was 3 mL min^{-1}; 400 W Xe lamp in the UV range (250–388 nm), 19.6 mW cm^{-1}	Selective formation of CH_4 as a main product with a yield of 1361 µmol g^{-1} h^{-1}	[60]
	0.2 wt% Au-P25	Impregnation precipitation	0.031 g. L^{-1} catalyst with medium-pressure Hg vapour lamp with a range of emission 254 ≤ λ ≤ 364 nm	HCOOH, CO and H_2 were reported as a main products with productivity of 6980, 84 and 2018 µmol. g^{-1} h^{-1}	This work
Semiconductor Systems	Rutile TiO_2 nanoparticle modified anatase TiO2 nanorods (TiO_2-RMA)	Synthesis	A 300 W mercury lamp	The total yield of CH_4 was 2.36 µmol. g^{-1} h^{-1}	[61]
	CoPc-TiO_2 (CoPc loaded titania)	improved sol–gel method using a homogeneous hydrolysis technique	500 W tungsten–halogen lamp	Total conversion of CO_2 was 34 µmol g^{-1} h^{-1} with HCOOH (28 µmol g^{-1} h^{-1}) as a main product.	[62]
	Cu-TiO_2	Sol–gel proces		CH_3OH yield under the UVC (254 nm) irradiation, was 600 µmol g_{cat}^{-1}. Switching to UVA (365 nm) resulted in a significant decrease of methanol yield in the range of 10 µmol g_{cat}^{-1}	[63]

Cu-TiO_2	Sol–gel method using a homogeneous hydrolysis technique	In aqueous solution using 254 nm UV irradiation, The optimum amount of copper loading was 2.0 wt%	CH_3OH 19.6 µmol g^{-1} h^{-1} after 6 h of UV illumination	[64]
TiO_2 powder		0.8 g L^{-1} TiO_2 powder with CO_2 up to 9 MPa with Xe lamp 990 W, and the light intensity of 0.96 kW m^{-2} for 5 h	Maximum productivity was HCOOH about 1.8 µmol g^{-1} h^{-1}	[65]
Rh-TiO_2	Impregnation method	Gas phase photoreaction: A mixture of CO_2 (150 mmol) and H_2 (50 mmol) was admitted to the reactor up to total pressure of 25 kPa. A 500 W ultrahigh-pressure mercury lamp was used in the bottom of reactor	Maximum productivity was CO/CH_4 5.2 µmol g^{-1} h^{-1}	[66]
P25		The TiO_2 powders suspended in iso-propyl alcohol solution as a hole scavenger and were irradiated with a Xe lamp.	CH_4 productivity in the optimum condition 1.3 µmol g^{-1}	[67]
P25		0.031 g L^{-1} catalyst with medium-pressure Hg vapour lamp with a range of emission 254 ≤ λ ≤ 364 nm	HCOOH and H_2 were reported as a main products with productivity of 4499 and 4000 µmol g^{-1} h^{-1}	This work
FSP	Flame spray pyrolysis	0.031 g L^{-1} catalyst with medium-pressure Hg vapour lamp with a range of emission 254 ≤ λ ≤ 364 nm	HCOOH and H_2 were reported as a main products with productivity of 7433 and 1613 µmol g^{-1} h^{-1}	This work

4 Conclusions

The high pressure photoreduction of CO_2 in water has been studied under different operating conditions, investigating the role of catalyst concentration, varying the amount of hole scavenger and the effect of adding gold on productivity and selectivity. A comparison between different flame-based techniques for the preparation of TiO_2 was also done, *i.e.* TiO_2 prepared by FSP and P25.

The hole scavenger plays a crucial role in the selective formation of gas products (CO and H_2) in the course of reaction time. In the presence of HS, photoreduction has been obtained in the liquid phase by formation of HCOOH as a main product. The consumption of the HS, instead, results in the consecutive photoreforming of the organic compounds accumulated in the liquid phase, with formation of secondary products, H_2 and CO, in the gas phase.

0.2 wt%-Au-P25 and TiO_2-FSP showed higher productivity for HCOOH with respect to TiO_2-P25. The method of synthesizing FSP nanoparticles may results in formation of metastable phase and defects which can further enhance the electron-hole pair generation and increasing the lifetime of photogenerated charges. Instead, the surface Plasmon resonance effect by doping Au on P25 can be considered as a man reason for higher HCOOH productivity in the presence of 0.2 wt%-Au-P25, with respect to bare TiO_2 P25.

Overall, appreciable amounts of energy per unit time have been stored through this reaction. The operating conditions should be tuned in order to drive the reaction towards the maximization of energy storage (high catalyst and HS concentrations) or the selection of the desired products.

Acknowledgements

The valuable help of the graduating student M. Ferrando is gratefully acknowledged.

I. Rossetti and E. Bahadori are grateful to Fondazione Cariplo and Regione Lombardia for financial support through the grant 2016-0858 – "Up-Unconventional Photoreactors".

The financial contribution of MIUR through the PRIN2015 grant (20153T4REF) is gratefully acknowledged (G. Ramis and I. Rossetti).

5 References

[1] G. Centi, S. Perathoner, Opportunities and prospects in the chemical recycling of carbon dioxide to fuels, Catal. Today. 148 (2009) 191–205. doi:10.1016/j.cattod.2009.07.075.

[2] G.P. Jessop, T. Ikariya, R. Noyori, © 19 9 4 Nature Publishing Group, Nature. 368 (1994) 231–233.

[3] A.A. Olajire, Valorization of greenhouse carbon dioxide emissions into value-added products by catalytic processes, J. CO2 Util. 3–4 (2013) 74–92. doi:10.1016/j.jcou.2013.10.004.

[4] W. Wang, J. Soulis, Y.J. Yang, P. Biswas, Comparison of CO 2 Photoreduction Systems : A Review, (2014) 533–549. doi:10.4209/aaqr.2013.09.0283.

[5] L. Yuan, Y.-J. Xu, Photocatalytic conversion of CO 2 into value-added and renewable fuels, Appl. Surf. Sci. 342 (2015) 154–167. doi:10.1016/j.apsusc.2015.03.050.

[6] A.L. Linsebigler, G. Lu, J.T. Yates, Photocatalysis on TiOn Surfaces: Principles, Mechanisms, and Selected Results, (1995) 735–758. doi:10.1021/cr00035a013.

[7] X. Li, J. Wen, J. Low, Y. Fang, J. Yu, Design and fabrication of semiconductor photocatalyst for photocatalytic reduction of CO 2 to solar fuel, 2014. doi:10.1007/s40843-014-0003-1.

[8] X. Chang, T. Wang, P. Zhang, J. Zhang, A. Li, J. Gong, Enhanced Surface Reaction Kinetics and Charge Separation of p − n, (2015) 3–6. doi:10.1021/jacs.5b04186.

[9] Q. Zhai, S. Xie, W. Fan, Q. Zhang, Y. Wang, W. Deng, Y. Wang, Angewandte Photocatalytic Conversion of Carbon Dioxide with Water into Methane : Platinum and Copper (I) Oxide Co-catalysts with a Core – Shell Structure **, (2013) 5776–5779. doi:10.1002/anie.201301473.

[10] J.L. White, M.F. Baruch, J.E. Pander, Y. Hu, I.C. Fortmeyer, J.E. Park, T. Zhang, K. Liao, J. Gu, Y. Yan, T.W. Shaw, E. Abelev, A.B. Bocarsly, Light-Driven Heterogeneous Reduction of Carbon Dioxide : Photocatalysts and Photoelectrodes, (2015). doi:10.1021/acs.chemrev.5b00370.

[11] S.N. Habisreutinger, L. Schmidt-Mende, J.K. Stolarczyk, Photocatalytic reduction of CO2 on TiO2 and other semiconductors, Angew. Chemie - Int. Ed. 52 (2013) 7372–7408. doi:10.1002/anie.201207199.

[12] S. Xie, Q. Zhang, G. Liu, Y. Wang, Photocatalytic and photoelectrocatalytic reduction of

CO2 using heterogeneous catalysts with controlled nanostructures, Chem. Commun. 52 (2015) 35–59. doi:10.1039/C5CC07613G.

[13] Y. Ma, X. Wang, Y. Jia, X. Chen, H. Han, C. Li, Titanium Dioxide-Based Nanomaterials for Photocatalytic Fuel Generations, Chem. Rev. 114 (2014) 9987–10043. doi:10.1021/cr500008u.

[14] V.P. Indrakanti, J.D. Kubicki, H.H. Schobert, Photoinduced activation of CO2 on Ti-based heterogeneous catalysts: Current state, chemical physics-based insights and outlook, Energy Environ. Sci. 2 (2009) 745. doi:10.1039/b822176f.

[15] M. Gattrell, N. Gupta, A. Co, A review of the aqueous electrochemical reduction of CO2 to hydrocarbons at copper, J. Electroanal. Chem. 594 (2006) 1–19. doi:10.1016/j.jelechem.2006.05.013.

[16] B. Michalkiewicz, J. Majewska, G. Ka, K. Bubacz, S. Mozia, A.W. Morawski, Reduction of CO2 by adsorption and reaction on surface of TiO2 -nitrogen modified photocatalyst, J. CO2 Util. 5 (2014) 47–52. doi:10.1016/j.jcou.2013.12.004.

[17] Y. Izumi, Recent advances (2012-2015) in the photocatalytic conversion of carbon dioxide to fuels using solar energy: Feasibilty for a new energy, ACS Symp. Ser. 1194 (2015) 1–46. doi:10.1021/bk-2015-1194.ch001.

[18] H. He, P. Zapol, L.A. Curtiss, A Theoretical Study of CO2 Anions on Anatase (101) Surface, J. Phys. Chem. C. 114 (2010) 21474–21481.

[19] H. He, P. Zapol, L.A. Curtiss, Computational screening of dopants for photocatalytic two-electron reduction of CO2 on anatase (101) surfaces, Energy Environ. Sci. 5 (2012) 6196–6205. doi:10.1039/c2ee02665a.

[20] B.-R. Chen, V.-H. Nguyen, J.C.S. Wu, R. Martin, K. Kočí, Production of renewable fuels by the photohydrogenation of CO2: effect of the Cu species loaded onto TiO2 photocatalysts., Phys. Chem. Chem. Phys. 18 (2016) 4942–51. doi:10.1039/c5cp06999h.

[21] K. Koci, K. Matteju, L. Obalovà, S. Krejcikovà, Z. Lacny, D. Plachà, L. Capek, A. Hospodkovà, O. Solcovà, Effect of silver doping on the TiO2 for photocatalytic reduction of CO2, Appl. Catal. B Environ. 96 (2010) 239–244. doi:10.1016/j.apcatb.2010.02.030.

[22] K. Li, X. An, K.H. Park, M. Khraisheh, J. Tang, A critical review of CO2 photoconversion: Catalysts and reactors, Catal. Today. 224 (2014) 3–12. doi:10.1016/j.cattod.2013.12.006.

[23] X. Chen, S. Shen, L. Guo, S.S. Mao, Semiconductor-based Photocatalytic Hydrogen

Generation, Chem. Rev. 110 (2010) 6503–6570. doi:10.1021/cr1001645.

[24] I. Rossetti, A. Villa, M. Compagnoni, L. Prati, G. Ramis, C. Pirola, C.L. Bianchi, W. Wang, D. Wang, CO2 photoconversion to fuels under high pressure: effect of TiO2 phase and of unconventional reaction conditions, Catal. Sci. Technol. 5 (2015) 4481–4487. doi:10.1039/C5CY00756A.

[25] I. Rossetti, A. Villa, C. Pirola, L. Prati, G. Ramis, A novel high-pressure photoreactor for CO2 photoconversion to fuels, RSC Adv. 4 (2014) 28883–28885. doi:10.1039/c4ra03751k.

[26] A. Olivo, E. Ghedini, M. Signoretto, M. Compagnoni, I. Rossetti, Liquid vs. Gas Phase CO2 Photoreduction Process: Which Is the Effect of the Reaction Medium?, Energies. 10 (2017) 1394. doi:10.3390/en10091394.

[27] I. Rossetti, E. Bahadori, A. Tripodi, A. Villa, L. Prati, G. Ramis, Conceptual design and feasibility assessment of photoreactors for solar energy storage, Sol. Energy. in press (n.d.). doi:https://doi.org/10.1016/j.solener.2018.02.056.

[28] M. Compagnoni, J. Lasso, A.I. Di Michele, I. Rossetti, Catalysis Science & Technology Flame-pyrolysis-prepared catalysts for the steam reforming of ethanol, Catal. Sci. Technol. 6 (2016) 6247–6256. doi:10.1039/C5CY01958C.

[29] G.L. Chiarello, I. Rossetti, L. Forni, Flame-spray pyrolysis preparation of perovskites for methane catalytic combustion, J. Catal. 236 (2005) 251–261.

[30] M. Compagnoni, S.A. Kondrat, C.E.E. Chan-Thaw, D.J. Morgan, D. Wang, L. Prati, N. Dimitratos, I. Rossetti, Spectroscopic Investigation of Titania Supported Gold Nanoparticles Prepared by a Modified DP Method for the Oxidation of CO, ChemCatChem. 8 (2016) 12.

[31] M. Compagnoni, E. Bahdori, A. Tripodi, A. Villa, C. Pirola, L. Prati, G. Ramis, N. Dimitratos, D. Wang, I. Rossetti, High Pressure CO2 Photoreduction using Au/TiO2: unravelling the effect of the co-catalyst and of the titania polymorph, Appl. Catal. B Environ. submitted (n.d.).

[32] F. Galli, M. Compagnoni, D. Vitali, C. Pirola, C.L. Bianchi, A. Villa, L. Prati, I. Rossetti, CO2 photoreduction at high pressure to both gas and liquid products over titanium dioxide, Appl. Catal. B Environ. 200 (2017) 386–391. doi:10.1016/j.apcatb.2016.07.038.

[33] M. Compagnoni, G. Ramis, F.S. Freyria, M. Armandi, B. Bonelli, I. Rossetti, Innovative photoreactors for unconventional photocatalytic processes: the photoreduction of CO2 and

the photo-oxidation of ammonia, Rend. Lincei. 28 (2017) S151. doi:10.1007/s12210-017-0617-z.

[34] K. Thamaphat, P. Limsuwan, B. Ngotawornchai, Phase Characterization of TiO 2 Powder by XRD and TEM, 361 (2008) 357–361.

[35] R.A. Spurr, H. Myers, Quantitative Analysis of Anatase-Rutile Mixtures with an X-Ray Diffractometer, (n.d.) 760–762. doi:10.1021/ac60125a006.

[36] R. Chauhan, A. Kumar, R.P. Chaudhary, Structural and optical characterization of Ag-doped TiO 2 nanoparticles prepared by a sol – gel method, (2012) 1443–1453. doi:10.1007/s11164-011-0475-8.

[37] M. Thommes, K. Kaneko, A. V Neimark, J.P. Olivier, F. Rodriguez-reinoso, J. Rouquerol, K.S.W. Sing, Physisorption of gases , with special reference to the evaluation of surface area and pore size distribution (IUPAC Technical Report), 87 (2015) 1051–1069. doi:10.1515/pac-2014-1117.

[38] N. Seifvand, E. Kowsari, Synthesis of Mesoporous Pd-Doped TiO2 Templated by a Magnetic Recyclable Ionic Liquid for Efficient Photocatalytic Air Treatment, Ind. Eng. Chem. Res. 55 (2016) 10533–10543.

[39] S. Tan, B.. Chen, W. Sun, X, W.J. Fan, H.S. Kwok, X.H. Zhang, Blueshift of optical band gap in ZnO thin films grown by metal-organic chemical-vapor deposition, J. Appl. Phys. 98 (2005) 013505.

[40] P. Li, H. Hu, J. Xu, H. Jing, H. Peng, J. Lu, New insights into the photo-enhanced electrocatalytic reduction of carbon dioxide on MoS2-rods/TiO2 NTs with unmatched energy band, Appl. Catal., B Env. 147 (2014) 912–919.

[41] S.I. Mogal, V.G. Gandhi, M. Mishra, S. Tripathi, T. Shripathi, P.. Joshi, D. O. shah, Single-Step Synthesis of Silver-Doped Titanium Dioxide: Influence of Silver on Structural, Textural, and Photocatalytic Properties, Ind. Eng. Chem. Res. 53 (2014) 5749–5758.

[42] Y. Izumi, Recent advances in the photocatalytic conversion of carbon dioxide to fuels with water and/or hydrogen using solar energy and beyond, Coord. Chem. Rev. 257 (n.d.) 171–186.

[43] C.H. Ao, S.C. Lee, J.Z. Yu, J.H. Xu, Photodegradation of formaldehyde by photocatalyst TiO2: effects on the presences of NO, SO2 and VOCs, Appl. Catal. B Environ. 54 (2004) 41–50. doi:10.1016/j.apcatb.2004.06.004.

[44] J. Shen, R. Kortlever, R. Kas, Y.Y. Birdja, O. Diaz-morales, Y. Kwon, I. Ledezma-yanez, K.J.P. Schouten, G. Mul, M.T.M. Koper, Electrocatalytic reduction of carbon dioxide to carbon monoxide and methane at an immobilized cobalt, Nat. Commun. 6 (2015) 1–8. doi:10.1038/ncomms9177.

[45] Z. Weng, J. Jiang, Y. Wu, Z. Wu, X. Guo, K.L. Materna, W. Liu, V.S. Batista, G.W. Brudvig, H. Wang, Electrochemical CO2 Reduction to Hydrocarbons on a Heterogeneous Molecular Cu Catalyst in Aqueous Solution, J. AM. CHEM. SOC. 138 (2016) 8076–8079.

[46] K. Manthiram, B.J. Beberwyck, A.P. Alivisatos, Enhanced Electrochemical Methanation of Carbon Dioxide with a Dispersible Nanoscale Copper Catalyst, 136 (2014) 13319–13325.

[47] M.S. Xie, B.Y. Xia, Y. Li, Y. Yan, Y. Yang, Q. Sun, S.H. Chan, A. Fishere, X. Wang, Amino acid modified copper electrodes for the enhanced selective electroreduction of carbon dioxide towards hydrocarbons, Energy Environ. Sci. 9 (2016) 1687–1695.

[48] K. Kočí, L. Obalová, L. Matějová, D. Plachá, Z. Lacný, J. Jirkovský, O. Šolcová, Effect of TiO2 particle size on the photocatalytic reduction of CO2, Appl. Catal. B Environ. 89 (2009) 494–502. doi:10.1016/j.apcatb.2009.01.010.

[49] W.Y. Teoh, A Perspective on the Flame Spray Synthesis of Photocatalyst Nanoparticles, (2013) 3194–3212. doi:10.3390/ma6083194.

[50] L. Bettini, M. Diamanti, M. Sansotera, M. Pedeferri, W. Navarrini, P. Milani, Immobilized TiO 2 nanoparticles produced by flame spray for photocatalytic water remediation, J. Nanoparticle Res. 18 (2016) 238. doi:10.1007/s11051-016-3551-6.

[51] L. Bettini, M. Dozzi, F. Della Foglia, G. Chiarello, E. Selli, C. Lenardi, P. Piseri, P. Milani, Mixed-phase nanocrystalline TiO2 photocatalysts produced by flame spray pyrolysis, Appl. Catal. B, Environ. 178 (2015) 226. doi:10.1016/j.apcatb.2014.09.013.

[52] W. Hou, W.H. Hung, P. Pavaskar, A. Goeppert, M. Aykol, S.B. Cronin, Photocatalytic conversion of CO2 to hydrocarbon fuels via plasmon-enhanced absorption and metallic interband transitions, ACS Catal. 1 (2011) 929–936. doi:10.1021/cs2001434.

[53] J. Yu, J. Low, W. Xiao, P. Zhou, M. Jaroniec, Enhanced Photocatalytic CO 2 - Reduction Activity of Anatase TiO 2 by Coexposed {001} and {101} Facets, (2014) 8839–8842. doi:10.1021/ja5044787.

[54] L. Liu, C. Zhao, Y. Li, Spontaneous Dissociation of CO 2 to CO on Defective Surface of Cu (I)/ TiO 2 − x Nanoparticles at Room Temperature, J. Phys. Chem. C 2012,. 116 (2012).

doi:10.1021/jp300932b.

[55] X. Meng, S. Ouyang, T. Kako, P. Li, Q. Yu, T. Wang, J. Ye, TiO 2 without loading noble metal cocatalyst †, Chem. Commun. 50 (2014) 11517–11519. doi:10.1039/C4CC04848B.

[56] S. Xie, Y. Wang, Q. Zhang, W. Fan, W. Deng, Y. Wang, Photocatalytic reduction of CO2 with H2O: significant enhancement of the activity of Pt–TiO2 in CH4 formation by addition of MgO†, Chem. Commun. 49 (2013) 2451–2453. doi:10.1039/c3cc00107e.

[57] Y. Liao, S. Cao, Y. Yuan, Q. Gu, Z. Zhang, C. Xue, Efficient CO 2 Capture and Photoreduction by Amine-, Chem. Eur. J. 20 (2014) 10220–10222. doi:10.1002/chem.201403321.

[58] H.W. Nasution, E. Purnama, S. Kosela, J. Gunlazuardi, Photocatalytic reduction of CO2 on copper-doped Titania catalysts prepared by improved-impregnation method, Catal. Commun. 6 (2005) 313–319. doi:10.1016/j.catcom.2005.01.011.

[59] O. Ishitani, C. Inoue, Y. Suzuki, T. Ibusuki, Photocatalytic reduction of carbon dioxide to methane and acetic acid by an aqueous suspension of metal-deposited TiO2, J. Photochem. Photobiol. A Chem. 72 (1993) 269–271.

[60] W. Wang, W. An, B. Ramalingam, S. Mukherjee, D.M. Niedzwiedzki, S. Gangopadhyay, P. Biswas, Size and Structure Matter: Enhanced CO 2 Photoreduction E ffi ciency by Size-Resolved Ultra fi ne Pt Nanoparticles on TiO 2 Single Crystals, J. Am. Chem. Soc. 134 (2012) 11276–11281. doi:10.1021/ja304075b.

[61] P.Q. Wang, Y. Bai, J.Y. Liu, Z. Fan, Y.Q. Hu, One-pot synthesis of rutile TiO2 nanoparticle modified anatase TiO2 nanorods toward enhanced photocatalytic reduction of CO 2 into hydrocarbon fuels, Catal. Commun. 29 (2012) 185–188. doi:10.1016/j.catcom.2012.10.010.

[62] S. Liu, Z. Zhao, Z. Wang, Photocatalytic reduction of carbon dioxide using sol – gel derived titania-supported CoPc catalysts, Photochem. Photobiol. Sci. 6 (2007) 695–700. doi:10.1039/b613098d.

[63] I.-H. Tseng, J.C.S. Wu, H.-Y. Chou, Effects of sol–gel procedures on the photocatalysis of Cu/TiO2 in CO2 photoreduction, J. Catal. 221 (2004) 432–440.

[64] I.-H. Tseng, W.-C. Chang, J.C.S. Wu, Photoreduction of CO2 using sol–gel derived titania and titania-supported copper catalystsNo Title, Environ. Appl. Catal. B. 37 (2002) 37–48.

[65] S. Kaneco, H. Kurimoto, Y. Shimizu, K. Ohta, Photocatalytic reduction of CO 2 using TiO 2 powders in supercritical fluid CO 2, Energy. 24 (1999) 21–30.

[66] Y. Kohno, H. Hayashi, S. Takenaka, T. Tanaka, T. Funabiki, S. Yoshida, Photo-enhanced reduction of carbon dioxide with hydrogen over Rh / TiO 2, 126 (1999) 117–123.

[67] S. Kaneco, Y. Shimizu, K. Ohta, T. Mizuno, Photocatalytic reduction of high pressure carbon dioxide using TiO2 powders with a positive hole scavenger, J. Photochem. Photobiol. A Chem. 115 (1998) 223–226.